

# Iron in Alzheimer's Disease: Analysis of the UK Biobank Dataset

*Laurance Lau*

Electrical Engineering and Computer Sciences  
University of California, Berkeley

Technical Report No. UCB/EECS-2024-25

<http://www2.eecs.berkeley.edu/Pubs/TechRpts/2024/EECS-2024-25.html>

April 30, 2024



Copyright © 2024, by the author(s).  
All rights reserved.

Permission to make digital or hard copies of all or part of this work for personal or classroom use is granted without fee provided that copies are not made or distributed for profit or commercial advantage and that copies bear this notice and the full citation on the first page. To copy otherwise, to republish, to post on servers or to redistribute to lists, requires prior specific permission.

### Acknowledgement

I would like to thank my advisor Chunlei Liu for his generous support, Zoe Cohen for her patient guidance, and Sang Min Han for our enlightening conversations. I would also like to thank Professor Miki Lustig for sharing the computational resources of his lab and taking the time to read this thesis.

---

# Iron in Alzheimer's Disease: Analysis of the UK Biobank Dataset

by Laurance Lau

---

## Research Project

Submitted to the Department of Electrical Engineering and Computer Sciences,  
University of California at Berkeley, in partial satisfaction of the requirements for the  
degree of **Master of Science, Plan II**.

Approval for the Report and Comprehensive Examination:

### Committee:



---

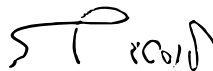
Professor Chunlei Liu  
Research Advisor

04/30/2024

---

(Date)

\* \* \* \* \*



---

Professor Michael Lustig  
Second Reader

04/30/2024

---

(Date)

## Abstract

Iron in Alzheimer's Disease: Analysis of the UK Biobank Dataset

by

Laurance Lau

Master of Science in Computer Science

University of California, Berkeley

Professor Chunlei Liu, Chair

A growing body of evidence suggests that iron deposition in the brain contributes to neurodegeneration. We use this as motivation to analyze the dietary and brain imaging data of UK Biobank and explore their connections to Alzheimer's disease (AD). We use decision tree and logistic regression models to predict AD incidence and describe a pipeline for analyzing brain imaging data, using quantitative susceptibility mapping (QSM) to infer iron concentrations in the brain. We find no evidence linking diet to AD incidence and find significantly higher QSM of the deep gray matter regions overall in participants with AD.

# Contents

<b>Contents</b>	<b>i</b>
<b>1 Introduction</b>	<b>1</b>
<b>2 UK Biobank</b>	<b>2</b>
2.1 Overview . . . . .	2
2.2 Cohort Characteristics . . . . .	3
2.3 Medical History Data . . . . .	4
2.4 Dataset Features . . . . .	5
<b>3 Analysis of Dietary Data</b>	<b>7</b>
3.1 Motivations . . . . .	7
3.2 Dataset Description . . . . .	7
3.3 Methodology . . . . .	10
3.4 Results . . . . .	12
3.5 Discussion . . . . .	14
<b>4 Analysis of Brain Imaging Data</b>	<b>15</b>
4.1 Motivations . . . . .	15
4.2 Dataset Description . . . . .	15
4.3 Image Processing . . . . .	16
4.4 Methodology . . . . .	17
4.5 Results . . . . .	19
4.6 Discussion . . . . .	27
<b>5 Is There a Connection Between Diet and QSM?</b>	<b>28</b>
<b>6 Conclusion</b>	<b>32</b>
6.1 Future Work . . . . .	32
6.2 Iron in AD Pathology . . . . .	32
<b>Bibliography</b>	<b>33</b>

## Acknowledgments

I would like to thank my advisor Chunlei Liu for his generous support, Zoe Cohen for her patient guidance, and Sang Min Han for our enlightening conversations. I would also like to thank Professor Miki Lustig for sharing the computational resources of his lab and taking the time to read this thesis.

# Chapter 1

## Introduction

According to the National Institute of Aging, Alzheimer’s disease (AD) is the seventh leading cause of death in the United States and the most common cause of dementia among older adults ([40]). The etiology and pathology of AD has yet to be fully understood and a cure for AD remains elusive. Nonetheless, potential risk factors, ranging from genetic to lifestyle and environmental, have been identified. Since AD has no known cure and most cases are not hereditary, lifestyle choices that may relieve symptoms or positively impact prognosis are appealing avenues for research that may inspire preventative measures or provide alternatives to medical treatment.

We are interested in investigating the relationship between iron consumption, deposition, and AD as iron dyshomeostasis has emerged as a potential mechanism for inducing or exacerbating neurodegeneration. Iron dyshomeostasis is implicated in AD ([27, 35, 59]) and many other neurodegenerative diseases ([24, 26, 60]). Patients have been observed to exhibit elevated iron levels and iron deposition in specific areas of their brains ([1, 6, 19, 54]), a phenomenon associated with the severity of the condition ([5, 55]). Iron is redox-active and can catalyze the production of reactive oxygen species that contribute to oxidative stress ([12, 25]) and ferroptosis, an iron-dependent form of programmed cell death ([14]). The dysregulation of ferroptosis is theorized to lead to neurological disorders ([3, 58]). Further research in this direction may prove useful for developing novel treatments ([17, 41]).

Analyzing biomedical datasets may enable the discovery of new risk factors and hypothesis testing for established risk factors. One such dataset is UK Biobank, a large-scale study in the United Kingdom with over 500,000 participants. In this thesis, we analyze the dietary and brain imaging data of UK Biobank and explore their connections to AD.

# Chapter 2

## UK Biobank

### 2.1 Overview

UK Biobank is a large-scale cohort study involving participants aged 40–69 recruited in the United Kingdom between 2006 and 2010 ([52](#)). We retrieved the data in March 2023, at which time the UK Biobank cohort had 502,371 participants. The large number of participants enables follow-up studies of unprecedented scale and provides great statistical power for subsequent analyses.

Participants were invited to visit an assessment center on multiple occasions where they undergo a standardized procedure of data collection. All participants attended the initial assessment visit conducted between 2006 and 2010. A subset of participants attended additional assessments in the following years; around 20,000 participants attended the first repeat assessment conducted between 2012 and 2013, around 76,000 participants attended the imaging visit starting in 2014, and around 7,000 participants attended the first repeat imaging visit starting in 2019.

The data collection procedure is updated between assessment center visits. They generally involve the following stages: written consent, physical measurements, touchscreen questionnaires, and biological sample collection. During imaging visits, UK Biobank acquires scans of participants, including magnetic resonance imaging (MRI) scans of the brain.

UK Biobank also collects data outside of assessment center visits. For example, physical activity data is collected by inviting participants to wear an accelerometer for seven days and data on dietary habits and cognitive function is collected through optional web-based questionnaires. These questionnaires are sent to participants with an e-mail address and are accessible through the participant portal. The use of online questionnaires broadens the scope of data collection and relieves participants of the necessity of traveling to an assessment center at a specific time.



## 2.2 Cohort Characteristics

UK Biobank has apparent and well-documented selection biases based on the designated age range and location of its cohort. The age of participants at the time of the initial assessment visit ranges from 37 to 73 with a mean of 56.3. The vast majority of participants (88.2 % of all respondents) identify as ethnically British. Furthermore, the cohort exhibits an imbalance in biological sex (83.8 males to 100 females) that significantly differs from the national sex ratio reported in the 2011 UK census (96.3 males to 100 females) ([42]).

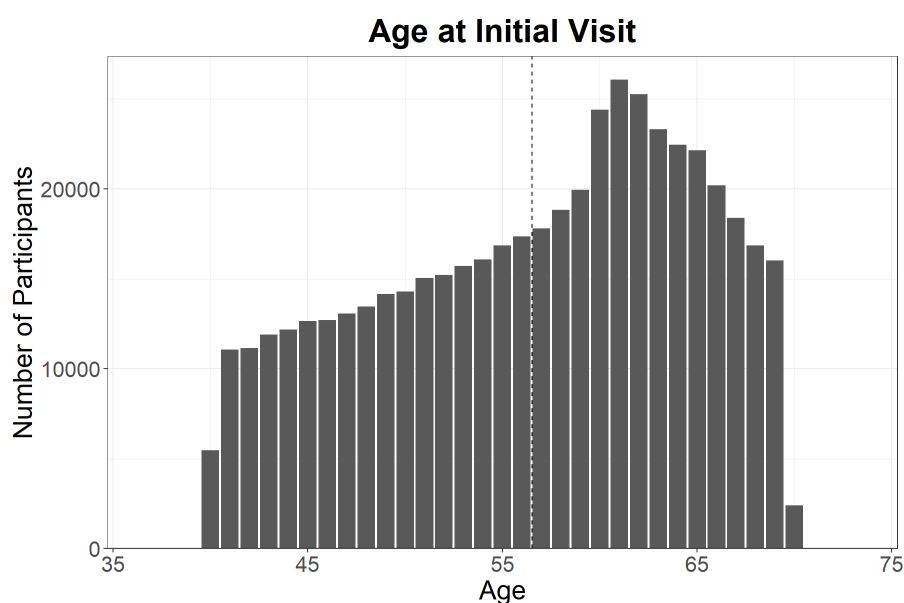


Figure 2.1: Age of UK Biobank participants at initial assessment visit (dashed — mean)

	White [British]	Asian*	Black	Mixed	Chinese*	Other response
Initial visit	472575 [442482]	9879	8058	2953	1573	6433
Repeat visit	19843 [18872]	137	95	76	44	139
1st imaging visit <sup>†</sup>	13632 [10755]	161	84	80	42	101
2nd imaging visit <sup>†</sup>	No data					

\*Chinese is considered separate from Asian following National Health Service convention

<sup>†</sup>Question removed from touchscreen questionnaire on 24th October 2016

Table 2.1: Ethnic background of UK Biobank participants

Health and socio-economic conditions affect one’s willingness to participate in time-consuming studies. UK Biobank exhibits a “healthy volunteer” selection bias ([16]); individuals who agreed to participate in the study tend to lead healthier lifestyles and be less socio-economically deprived. Similarly, those who returned for the first repeat assessment also tend to lead healthier lifestyles, be less socio-economically deprived, and be better educated compared to those who did not ([8]).

These biases undermine the conclusions we draw from this dataset since the cohort is not a representative sample of the UK population ([45]). Furthermore, the location of the study limits the generalizability of some results on a global scale. Similar biobank projects such as the All of Us Research Program in the United States and the H3Africa initiative in Africa are essential for validating results obtained using foreign data and generating findings specific to local demographics.

## 2.3 Medical History Data

Data from linked health records and physical measurements taken during the assessment center visits are available. Anonymity is achieved by hiding data fields with personally identifiable information such as home addresses from all researchers by default and only allowing researchers to interact with a unique ID number assigned to each participant.

Linked health records contain primary care data, hospital inpatient data, cancer data, and death data. All English and Welsh data are coded in ICD-10 for diagnoses and OPCS-4 for operations and procedures, while a portion of Scottish data is coded in the older versions of these codes, ICD-9 and OPCS-3.

UK Biobank has also collected information on self-reported medical conditions through verbal interviews. However, since AD has a complicated differential diagnosis and requires a physician to properly diagnose, I chose to rely on ICD-10 codes as the standard of determining whether someone has been afflicted with AD. I discarded all ICD-9 data since ICD-9 codes were there is only a single record of any kind of dementia (presenile dementia) and it is not specifically AD.

UK Biobank expected around 9,000 cases of AD to occur in its cohort by the year 2022 and around 30,000 cases by 2027 ([52]). There are actually 3,955 cases by the time of data retrieval (March 2023), which could be a manifestation of the “healthy volunteer” bias. This number shrinks when we specify subsetting criteria and exclude participants with missing data.

## 2.4 Dataset Features

The UK Biobank dataset has its strengths and limitations that affect the practicality of data analysis and the quality of the results. Some features are related to the organization of data storage while others concern particular types of data.

### Metadata

UK Biobank stores measurements and results in “Data-Fields”. These Data-Fields are categorized into broader collections known as “Categories” which can be Subcategories of another Category, creating a nested structure that makes searching for related Data-Fields easy.

Every Data-Field is given a descriptive title and has a high-level summary which is publicly available, including the number of records, histograms, and relevant statistics. Additional information about the data collection process is available for particular Categories. For example, the entire list of questions is provided for verbal interviews and questionnaires, and images of the computer interface are provided for cognitive testing tasks. This makes it easy to see at a glance whether a Data-Field or a Category may be useful.

### Redundant Data-Fields

There are seemingly redundant Data-Fields that do not serve a useful purpose. For example, there are two Data-Fields for year of birth (34, 22200) and four Data-Fields for body weight (3160, 12143, 21002, 23098). UK Biobank also notes that Data-Field 21002 “should be used in preference to” Data-Field 12143.

### Suspicious Multimodal Distributions

Multimodal distributions in continuous health data could be accounted for by different distributions due to biological sex (e.g. Data-Field 51: Seated height) or by subtle design in the assessment procedure (e.g. Data-Field 20015: Sitting height). However, rounding could be to blame for some occurrences, degrading the quality of the data. This likely explains multimodal distributions occurring in Data-Fields involving age responses (e.g. Data-Field 3680: Age when last ate meat).

## Handling Missing Data

The core dataset is organized in a relational model and is downloaded as a single file. Every participant is associated with all attributes regardless of whether they provided data for all of them. While relational databases have many advantages, this does not distinguish between an empty response or actual missing data. UK Biobank uses “Data-Codings” which provides additional codes for responses such as “Prefer not to say” or “Unknown” which distinguishes these from missing data.

Additional downloads are required for images and genetic data. Not every participant underwent scans because they may not have attended an imaging visit. Unfortunately, it is not possible to know the data availability of images until it is requested.

## Web-based Questionnaire

With the emergence of platforms such as Amazon Mechanical Turk and Prolific, online questionnaires have become a common and easy method of obtaining large amounts of responses quickly. However, the truthfulness of questionnaire responses cannot be guaranteed, especially if respondents experience fatigue from completing previous tasks or if the questionnaire takes too long. The 24-h dietary recall questionnaire has questions on around 200 foods and drinks; the mean time for completion is 17.7 minutes, with some participants taking as little as 5 minutes and some taking more than three hours. Later instances of the questionnaire are remotely completed without in-person support from UK Biobank staff. Even though later instances of the questionnaire are strictly optional, there is reason to question the quality of the responses.

Furthermore, in this thesis we are interested in AD which presents with short-term memory loss and cognitive deficit. Questionnaire responses received from participants with neurodegeneration should generally be taken with a grain of salt.

## Cognitive Battery

In figuring out how to determine whether a participant has cognitive deficits and to what degree, I looked into UK Biobank’s bespoke suite of 12 cognitive tests. Unfortunately, these tests are non-standard ([15]) and lack official documentation and it is unclear what cognitive domains these tests can assess. The burden of checking desirable properties such as validity and test-retest reliability and figuring out what cognitive ability these tests are assessing rests on the researchers using the data.

# Chapter 3

## Analysis of Dietary Data

### 3.1 Motivations

Iron is necessary for the proper functioning of various processes in the human body, and its imbalance is shown to be associated with diseases, some of which can be remedied by adjusting the amount of dietary iron intake. For example, iron-deficiency anemia can be treated with iron supplements, while patients with thalassemia are often advised to avoid iron in their diet.

With regard to neurology, iron deposition in the brain is linked to neurodegeneration, but there is scarce evidence linking iron consumption directly to iron deposition. It may seem naive to connect food consumption directly to neurological disease, but there exists conflicting research on whether a certain amount of iron intake increases the risk of developing neurodegeneration later in life ([36], [49]). Previous work done by Liu et al. using the 24-hour dietary recall questionnaire data from the UK Biobank dataset suggests that both deficient or excessive iron intake can contribute higher risk of developing dementia ([34]).

I am interested in discovering dietary determinants of AD. Can one's diet be predictive of the risk of developing AD? If so, which components of diet?

### 3.2 Dataset Description

UK Biobank conducted two parallel dietary assessments: a touchscreen questionnaire administered at the beginning of each assessment center visit and a web-based 24-hour dietary recall questionnaire ([32]). The latter includes questions on about 200 kinds of foods and additional questions on physical activity. Participants answered this questionnaire up to five times by invitation over a three year period between the initial and repeat assessment center visit. I primarily use data collected from the former, which includes 29 questions on dietary habits involving major food groups.

## Subsetting

At the time of data retrieval, the UK Biobank cohort consisted of 502,371 participants. Apart from excluding participants with missing data, I set exclusion criteria in order to better investigate the predictive power of diet on developing disease.

First, I excluded participants with an inconsistent diet. A participant has a consistent diet if they gave more “Yes” responses than “No” responses for Data-Field 100020, which indicates whether they had a typical diet the day prior answering the 24-hour dietary recall questionnaire, and if they never gave “Often” responses for Data-Field 1548, which indicates variation in diet when answering the touchscreen questionnaire.

Second, I excluded all participants who had ICD-9 codes but did not have ICD-10 codes. In order to determine whether someone develops AD or has other diseases, the hospital inpatient data in Category 2002 (Hospital inpatient: Summary Diagnoses) was used. UK Biobank provides both ICD-9 and the newer ICD-10 codes for medical diagnoses. I discovered that of all 20,390 participants using ICD-9 codes, only one participant has been diagnosed with any form of dementia. This is not only problematic for data analysis purposes because of the severe class imbalance and incompatibility with ICD-10 codes, but is also contradictory to the much higher frequency of dementia in older adults as stated in literature.

Third, I excluded all participants with an AD diagnosis at baseline. Since I want to investigate the predictive power of diet on AD incidence, it is not productive to include participants who already have AD at baseline because their diet has no bearing on the result. For convenience of data processing, I also exclude those who developed AD before their final assessment center visit.

Fourth, I excluded participants who passed away before developing AD because we never know if they would have developed AD had they stayed alive.

A total of 35 features comprising data from non-pilot Data-Fields in Category 100052 (Diet), Category 100058 (Smoking), Category 1001 (Primary demographics), and Category 100010 (Body size measures) was used. Any participant with missing data for any feature (including “Prefer not to answer” and “I don’t know” responses) was also excluded. Since plenty of data is available, simply excluding entries with missing data instead of imputation is preferable. The final sample had a total of 98,960 participants.

Of the entire sample, 50,780 are female and 48,180 are male; the vast majority had a British (90,965, 91.92%) or white (5,838, 5.90% Irish or other white background) ethnic background; the age at baseline ranged from 40 to 70 with a mean of 56.15; 283 (0.29 %) developed AD after attending all assessment visits.

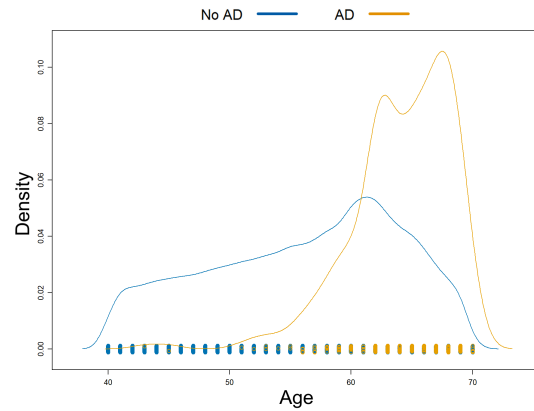


Figure 3.1: Smoothed age distribution of sampled participants at initial assessment visit

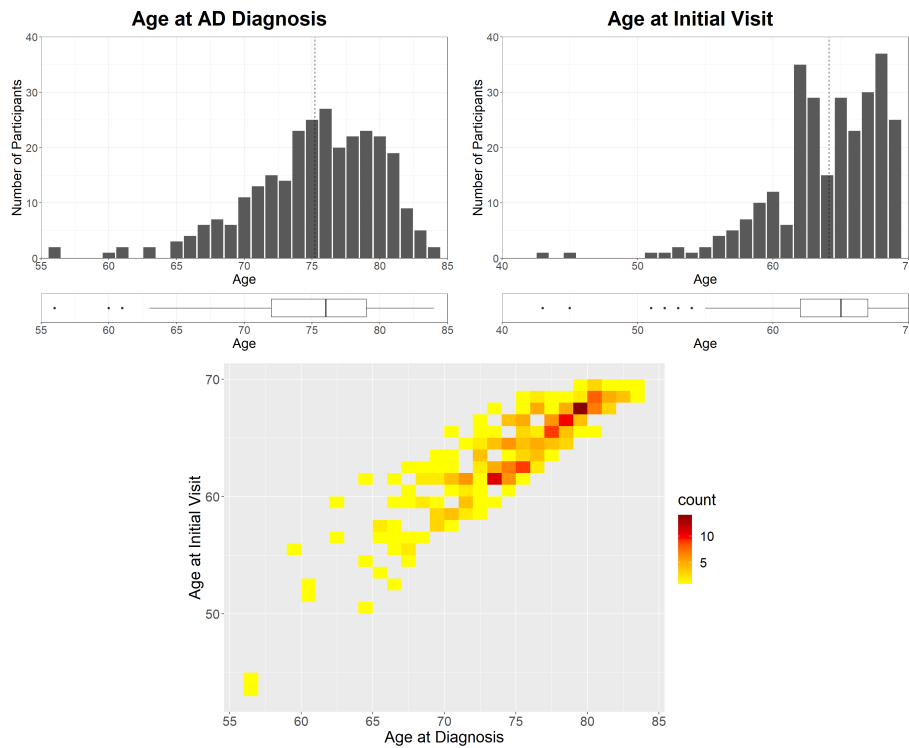


Figure 3.2: Age of sampled participants who developed AD. Top left: when they were diagnosed; top right: when they attended the initial assessment visit (dashed — mean). Bottom: combined age profile

Old age is a risk factor for AD. Of the participants in the sample who developed AD, the mean age when they received an AD diagnosis is 75.22 and the mean age when they attended the initial assessment visit is 64.14. Although these plots are based on the subset of data, they also reflect the general trend of participants in the entire cohort who have an AD diagnosis.

Although an investigation into dietary data is motivated by iron, it is inadequate to focus solely on iron intake because iron absorption is influenced by the consumption of other foods and drugs ([38, 44]). It is also possible that other nutrients and minerals also contribute to or suppress AD incidence, so it is reasonable to consider the full spectrum of foods for which data is available.

## 3.3 Methodology

### Data Processing

For each participant, I aggregated repeated responses to the same question by averaging responses across all assessment visits. Most of the questionnaire responses are discrete values that cannot be averaged directly but can be ranked in some sense, such as the frequency of consumption of foods. The data encoding provided by UK Biobank is used to convert these discrete responses into numerical values that can then be averaged. This aggregate value is used for the ensuing analyses.

### Model Selection

For each participant with a set of features, the goal is to predict a binary label denoting whether AD develops at the endpoint. To this end, I train logistic regression and decision tree models that attempt to predict AD incidence after a certain number of years from baseline in order to identify risk factors. I find these models to be appropriate in general for biomedical inquiries as their interpretability could be used to both reason about the model and inspire future work.

### Logistic Regression

Logistic regression is a popular method for binary classification. This model assumes that the features are linearly related to the log odds. Given features  $x$  and parameters  $\beta$ , the probability of a positive label  $P$  in this model is given by

$$P = \frac{1}{1 + \exp(-\beta^T x)}.$$

This model can be trained using maximum likelihood estimation (MLE) and optimization techniques such as gradient descent. As such, this has the additional benefits of MLE, including consistency and efficiency.



## Decision Trees

Decision tree models work with both discrete and continuous features and are interpretable and non-parametric. A single decision tree recursively partitions the feature space at each node with axis-aligned boundaries such that each resulting partition at the leaf nodes has a certain desired homogeneity of labels or the leaf node cannot be further split. The inhomogeneity of a set of labels is quantified by a concave measure such as entropy or Gini impurity. The optimal construction of decision trees is known to be NP-complete ([22]); in practice, it is workable to greedily maximize the information gain at each node. The R package `rpart` implements decision tree learning due to Breiman et al. ([10]).

## Random Forests

Decision trees are prone to severe overfitting because they can fit any function to any desired precision. Pruning, depth limiting, and relaxing the stopping homogeneity condition are techniques used to reduce the variance of decision trees. Random forests use two other techniques to achieve this: bootstrap aggregation (bagging), which involves training and averaging the output of many decision trees that each train on data that is resampled with replacement, and randomly choosing a subset of features to split on at each node. Bagging is guaranteed to be consistent if the underlying decision trees are consistent ([7]); random forests are guaranteed to converge ([9]) but are not known to be consistent ([7, 48, 53]). The R package `randomForest` implements Breiman's random forest algorithm.

## Data Analysis

MATLAB (version R2024a) was used for logistic regression. R (version 4.3.2) and libraries `caret`, `gbm`, `rpart`, `randomForest`, and `tidyverse` and their dependencies were used for data pre-processing and training decision tree models. The R library `ggplot2` and its dependencies were used to create figures.

A 80-20 train-test split was constructed with class ratios preserved. 5-fold cross-validation was performed for all types of models. Random forests were trained with 100, 300, and 1000 trees. 6 features were randomly chosen at each node; this is roughly the square root of the total number of features and is a recommendation attributed to Breiman ([20]). To do a finer search of parameter space, AdaBoost models were trained with cross-validation and a grid search on 20, 40, 60, 80, 100, 200, 400, or 600 trees, interaction depth 1, 0.002 or 0.005 shrinkage, and 1 or 10 minimum observations per leaf node. Logistic regression was also attempted.

I control for age and sex by repeating training with different brackets of age and sex. This may not be useful for decision tree models since these are capable of feature selection but this still helps to isolate the effects of old age and sex on AD incidence.

Depending on the accuracy of the model, variable importance plots can be used to interpret the effectiveness of splitting on individual features and partial dependence plots can be used to interpret how each individual variable affects the outcome.

## 3.4 Results

As few as 100 trees are sufficient to perfectly fit the training data. In the validation stage, all models uniformly classified all participants as negative for the eventual development of AD and failed to classify any participant as positive. That is, while all models achieved remarkable accuracy, they had zero sensitivity to eventual AD development.

However, we may still try to determine which of the individual variables have a greater effect on AD incidence. Plots of individual features suggested that high alcohol intake frequency may be a risk factor other than old age and did not suggest risk factors related to anthropometric measurements and other dietary items.

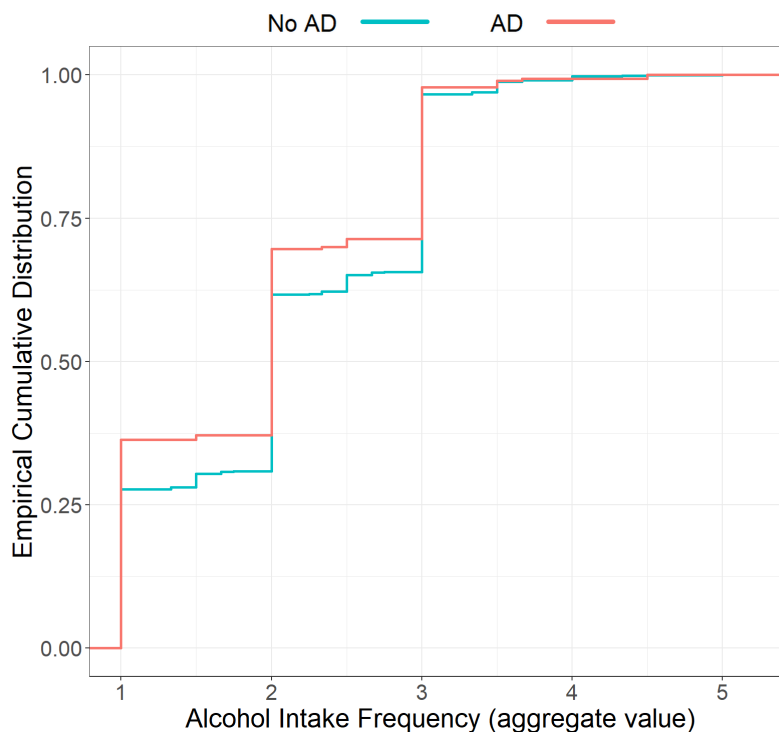


Figure 3.3: Alcohol intake frequency of sampled participants (lower number on the abscissa corresponds to higher frequency). Red: AD group; blue: no AD group

Model interpretation is meaningful when the models perform well to match the ground truth. Since the models have low sensitivity, we should cautiously interpret items that suggest a positive classification.

The Gini importance of a feature in random forest models is defined as the total decrease in Gini impurity from splitting on the feature averaged over all trees. The decision tree models generally find splitting on anthropometry measures and age to be more useful than splitting on dietary features.

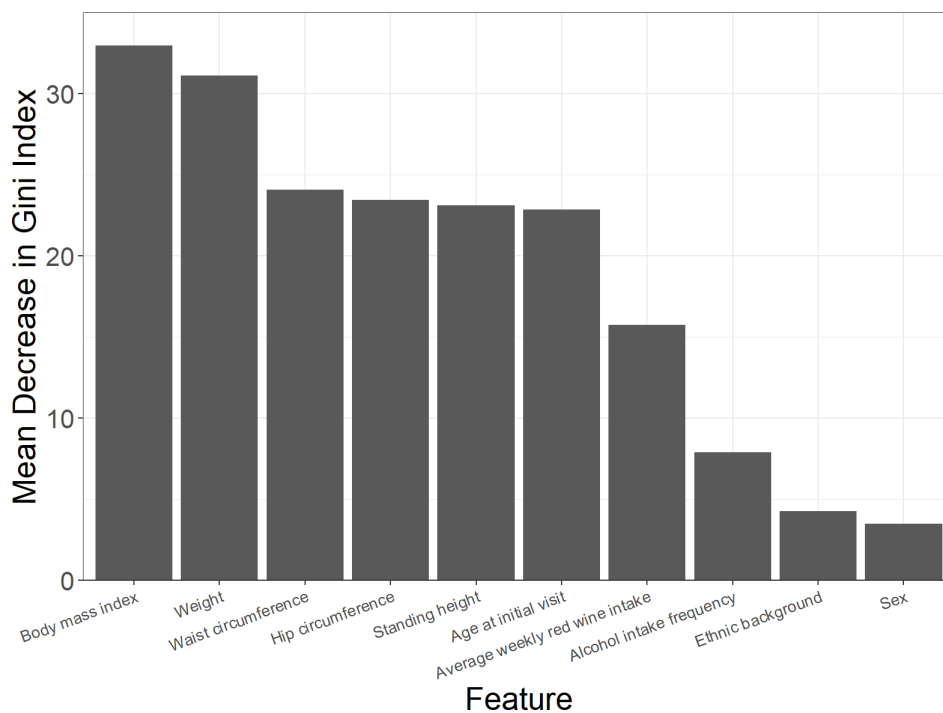


Figure 3.4: Gini importance plot of the top 10 features of a random forest with 1000 trees

We omit the partial dependence plots of the logistic regression model as most do not yield meaningful interpretations and some even display trends that contradict analyses on individual features. This is not surprising since logistic regression is sensitive to outliers and the model has a constant output that is supported by the most of the variables anyway.

## 3.5 Discussion

The results suggest that there is not enough information in the UK Biobank dietary survey included in the touchscreen questionnaire to predict AD incidence. There are many possible reasons for this outcome.

First, there may be too few positive labels for the models to learn from. This is an example of class imbalance in which the trained models simply ignore the minority group. One possible workaround is to oversample the minority group or to undersample the majority group, but we will no longer be modeling ground truth.

Second, the granularity of the dietary section of the touchscreen questionnaire may be insufficient, both in terms of the specificity of the foods included and in the discretized responses. Furthermore, it is not viable to quantify the consumption of particular nutrients of interest based on this data. We contrast this with the work done by Liu et al. mentioned in Section 3.1 where they find significant associations between iron consumption and all-cause dementia using a different Category of UK Biobank data which includes a much greater number of questions in much finer detail in addition to nutrition estimation data calculated by UK Biobank ([34, 43]).

Third, it is important to recognize that diet is only one out of many potential lifestyle and environmental risk factors for AD. Furthermore, there are many stages between food consumption and the development of disease that need to be examined carefully for a concrete connection to be established.

# Chapter 4

## Analysis of Brain Imaging Data

### 4.1 Motivations

Different biological tissues have different magnetic susceptibility. The magnetic resonance imaging (MRI) technique of quantitative susceptibility mapping (QSM) allows us to measure this property of brain tissues and infer the degree of iron deposition and myelination ([28, 33]). This is useful as iron deposition and demyelination are both observed in AD patients and both result in an increase in QSM signal.

We are interested in investigating the difference in the patterns of QSM signals between people with and without AD.

### 4.2 Dataset Description

We use brain imaging data from UK Biobank, which has been conducting its first phase of imaging assessment center visits since 2014 and a repeat phase since 2019 ([39, 50]). UK Biobank has the largest QSM dataset in existence ([57]).

The number of brain images of participants with AD is limited. Even though there are half a million participants in the entire study, around 76,000 participants attended the first imaging visit and 7,000 attended the repeat imaging visit. Furthermore, participants with an AD diagnosis are less likely to attend imaging visits and there are fewer of them than what UK Biobank expected.

58 participants with an AD diagnosis attended the first imaging visit and only one attended the repeat imaging visit. For this reason, we only use data collected during the first imaging visit. Participants whose images could not be processed through the pipeline described in the next section were excluded. In total, we used the susceptibility weighted brain images of 56 participants with an AD diagnosis and 945 participants without.

## Magnetic Resonance Imaging

MRI of the brain is commonly used to assess neurological abnormalities and in the diagnosis of AD which presents with brain atrophy that can be imaged with structural MRI. Some advantages of using MRI are its noninvasiveness and its many contrast mechanisms.

MRI utilizes the curious quantum mechanical phenomenon of nuclear magnetic resonance. The MRI machine generates a strong uniform magnetic field ( $B_0$ ), causing atomic nuclei inside the body to align with the field. A radiofrequency magnetic field ( $B_1$ ) is then applied and turned off, causing the nuclei to be misaligned momentarily. MRI measures the nuclear magnetism as the nuclei, typically single protons, realign with the  $B_0$  field.

## Quantitative Susceptibility Mapping

Magnetic susceptibility in tissues distorts the surrounding magnetic field. Since the precessional frequency of protons is proportional to the strength of the magnetic field, the protons precess at different rates as this distortion happens. Over time, a phase difference between photons emerges. We use this phase data from the susceptibility weighted brain MRI images which use a contrast mechanism that is particularly sensitive to magnetic susceptibility.

## 4.3 Image Processing

The phase data from the brain images are first converted into QSM signals before any statistical analysis is done. Even though UK Biobank has a QSM pipeline, implementing our own pipeline gives us more flexibility in handling the brain images ([2]).

### Image Reconstruction

A mask is generated using the Brain Extraction Tool provided by the FMRIB Software Library to separate the brain from the rest of the image ([23], [51]). The phase data is unwrapped using a Laplacian-based method and the background phase is removed using V-SHARP ([28], [46], [47]). We use these methods through their implementations provided by STI-Suite ([31]).

Reconstructing the QSM signal is a deconvolution problem where each point in the image contributes its own magnetic field distortion ([33]). As with all deconvolution problems, this is generally difficult and ill-posed, but many algorithms have been developed to attack the QSM reconstruction problem. We use the iLSQR and STAR-QSM algorithms provided by STI-Suite for image reconstruction ([29], [61]).

## Image Registration

Since the brains of each individual are different in shape and size, to figure out which part of the brain corresponds to which portion of the image and to perform statistical analysis using brains of different participants, we perform image registration to warp these images to a “standard” brain — a so-called ‘brain atlas’ with known labels. We use the symmetric normalization method provided by Advanced Normalization Tools together with an atlas made for QSM for image registration ([4, 63]).

## 4.4 Methodology

### Statistical Analysis

R is used for creating figures and MATLAB (version R2024a) is used for creating figures and all statistical analysis.

We compute the mean QSM signal for each of the regions of interest (ROIs) and compare the medians of the AD and non-AD groups using the Wilcoxon rank-sum test with the rank-biserial correlation ( $r_{rb}$ ) as the effect size.

It is known that QSM patterns change with age ([37, 56]). The AD group has a mean age of 70.4 while the non-AD group has a mean age of 65.5. We control for age by repeating the analysis using data only from participants within the 25th to 75th percentile of ages in the AD group (68 to 75 inclusive) for both groups. 29 participants with an AD diagnosis and 288 participants without an AD diagnosis were in this age range.

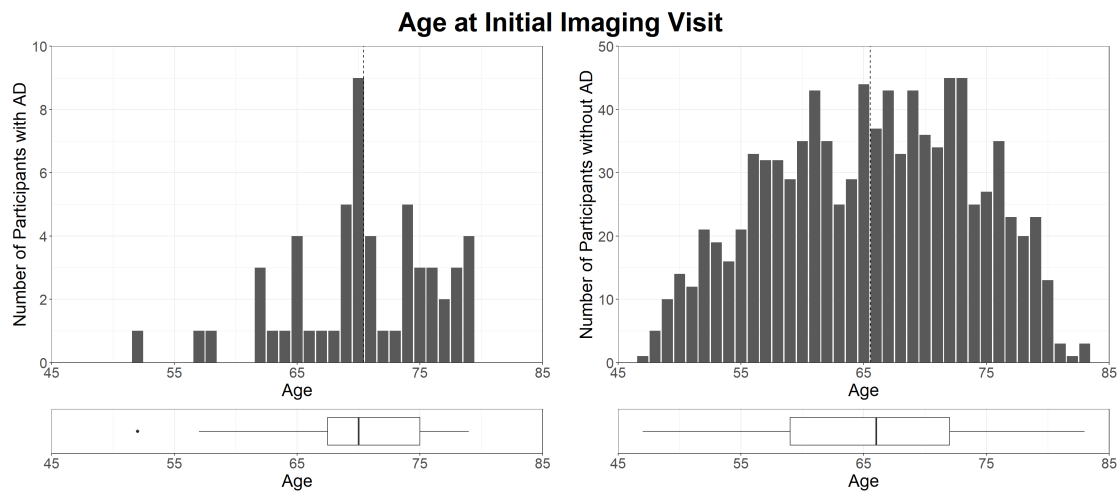


Figure 4.1: Age of sample participants at initial imaging visit (dashed — mean)

Furthermore, we investigate the effects of aging on QSM by considering the AD and non-AD groups separately and averaging the QSM of participants with the same age (rounded to the nearest year). One participant in the AD group with missing age data was excluded.

## Regions of Interest

It is known that QSM reflects iron deposition in deep gray matter regions where iron is concentrated, so we restrict our investigation to these regions. Deep gray matter regions are non-cortical gray matter regions, including the basal ganglia and surrounding regions such as the hippocampus and thalamus. This is a semantic designation based on anatomy and does not reflect the various functional roles these brain regions are responsible for.

Abbreviation	Region of Interest
Hip	Hippocampus
PHG	Parahippocampal gyrus
Amy	Amygdala
Put	Putamen
Cd	Caudate nucleus
Acb	Nucleus accumbens
EA	Extended amygdala
GPe	External globus pallidus
GPi	Internal globus pallidus
SNr	Pars reticulata of substantia nigra
SNC	Pars compacta of substantia nigra
RN	Red nucleus
STh	Subthalamic nucleus
VP	Ventral pallidum
ANG	Anterior nuclei of thalamus
MD	Median nuclei of thalamus
IML	Internal medullary lamina of thalamus
LNG	Lateral nuclei of thalamus
Pul	Pulvinar nuclei of thalamus
DN	Dentate nucleus

Table 4.1: Abbreviations of deep gray matter regions of interest



## 4.5 Results

### Comparison of AD and Non-AD Groups

We find significant differences between the QSM of the AD group and the non-AD group in deep gray matter regions. Except the amygdala, ANG, MD, IML, and LNG, the QSM of the deep gray matter regions is higher for the AD group compared to the non-AD group.

QSM does not differ greatly between iLSQR and STAR-QSM reconstructions. Similar patterns of differences between the AD and non-AD group are shared by the entire sample and the 68- to 75-year-old subset.

#### iLSQR Reconstruction

ROI	$p$ -value	$r_{rb}$	ROI	$p$ -value	$r_{rb}$
Hip <sub>L</sub>	$3.13 \times 10^{-9}$	0.187	SN <sub>C</sub> <sub>L</sub>	$3.25 \times 10^{-27}$	0.342
Hip <sub>R</sub>	$1.20 \times 10^{-9}$	0.192	SN <sub>C</sub> <sub>R</sub>	$6.99 \times 10^{-27}$	0.340
PHG <sub>L</sub>	0.996	-0.000165	RN <sub>L</sub>	$2.69 \times 10^{-29}$	0.355
PHG <sub>R</sub>	$6.90 \times 10^{-4}$	0.107	RN <sub>R</sub>	$1.08 \times 10^{-30}$	0.364
Amy <sub>L</sub>	$7.79 \times 10^{-35}$	-0.389	STh <sub>L</sub>	$6.45 \times 10^{-31}$	0.366
Amy <sub>R</sub>	$1.87 \times 10^{-29}$	-0.356	STh <sub>R</sub>	$4.38 \times 10^{-32}$	0.373
Put <sub>L</sub>	$3.29 \times 10^{-29}$	0.355	VP <sub>L</sub>	0.0400	0.0649
Put <sub>R</sub>	$8.02 \times 10^{-25}$	0.325	VP <sub>R</sub>	0.0914	0.0534
Cd <sub>L</sub>	$1.01 \times 10^{-17}$	0.271	ANG <sub>L</sub>	$4.45 \times 10^{-13}$	-0.229
Cd <sub>R</sub>	$7.28 \times 10^{-15}$	0.246	ANG <sub>R</sub>	$2.79 \times 10^{-8}$	-0.176
Acb <sub>L</sub>	0.0381	0.0656	MD <sub>L</sub>	0.0541	-0.0609
Acb <sub>R</sub>	$2.56 \times 10^{-7}$	0.163	MD <sub>R</sub>	$4.51 \times 10^{-3}$	-0.0898
EA <sub>L</sub>	$1.37 \times 10^{-29}$	0.357	IML <sub>L</sub>	$3.51 \times 10^{-9}$	-0.187
EA <sub>R</sub>	$1.67 \times 10^{-31}$	0.369	IML <sub>R</sub>	$1.24 \times 10^{-13}$	-0.234
GPe <sub>L</sub>	$4.60 \times 10^{-34}$	0.385	LNG <sub>L</sub>	$1.37 \times 10^{-27}$	-0.344
GPe <sub>R</sub>	$1.23 \times 10^{-33}$	0.382	LNG <sub>R</sub>	$1.01 \times 10^{-28}$	-0.352
GPI <sub>L</sub>	$1.26 \times 10^{-35}$	0.394	Pul <sub>L</sub>	0.154	0.0451
GPI <sub>R</sub>	$6.26 \times 10^{-35}$	0.390	Pul <sub>R</sub>	$1.71 \times 10^{-6}$	0.151
SN <sub>r</sub> <sub>L</sub>	$1.78 \times 10^{-29}$	0.357	DN <sub>L</sub>	$3.12 \times 10^{-20}$	0.291
SN <sub>r</sub> <sub>R</sub>	$4.96 \times 10^{-30}$	0.360	DN <sub>R</sub>	$0.41 \times 10^{-19}$	0.280

Table 4.2: Results of Wilcoxon rank-sum test on QSM data of AD and non-AD groups in deep gray matter regions reconstructed using iLSQR. L/R subscript denotes left or right side.  $r_{rb}$  is the rank-biserial correlation

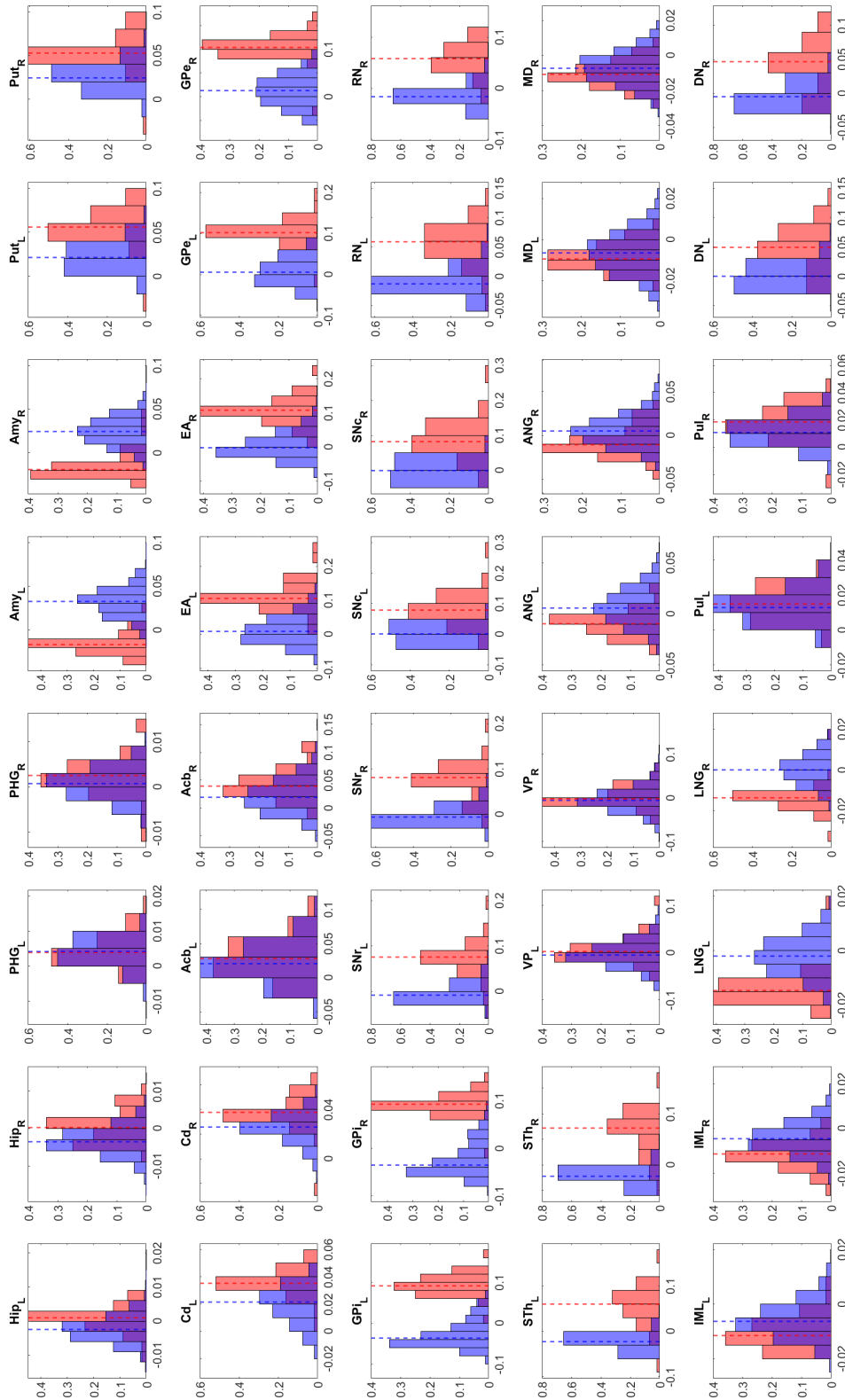


Figure 4.2: Proportion of participants with QSM signal in ppm (iLSQR reconstruction) in deep gray matter regions (Red: participants with AD diagnosis; blue: participants without AD diagnosis; dashed lines: medians of each group)

**STAR-QSM Reconstruction**

It is possible that these observations are due to inaccuracies in the reconstruction or registration processes. To be more confident that the results are not due to particulars of iLSQR reconstruction, we repeat the analysis with STAR-QSM reconstruction, which yields similar results.

ROI	$p$ -value	$r_{rb}$	ROI	$p$ -value	$r_{rb}$
Hip <sub>L</sub>	$1.79 \times 10^{-8}$	0.178	SN <sub>C<sub>L</sub></sub>	$2.35 \times 10^{-26}$	0.336
Hip <sub>R</sub>	$9.60 \times 10^{-7}$	0.155	SN <sub>C<sub>R</sub></sub>	$1.13 \times 10^{-28}$	0.351
PHG <sub>L</sub>	0.0628	0.0588	RN <sub>L</sub>	$3.86 \times 10^{-30}$	0.361
PHG <sub>R</sub>	$3.27 \times 10^{-5}$	0.131	RN <sub>R</sub>	$9.66 \times 10^{-33}$	0.377
Amy <sub>L</sub>	$4.63 \times 10^{-35}$	-0.391	STh <sub>L</sub>	$5.98 \times 10^{-30}$	0.360
Amy <sub>R</sub>	$8.19 \times 10^{-30}$	-0.359	STh <sub>R</sub>	$1.11 \times 10^{-31}$	0.370
Put <sub>L</sub>	$1.86 \times 10^{-30}$	0.363	VP <sub>L</sub>	0.411	0.0260
Put <sub>R</sub>	$2.67 \times 10^{-26}$	0.336	VP <sub>R</sub>	0.637	0.0149
Cd <sub>L</sub>	$4.21 \times 10^{-18}$	0.274	ANG <sub>L</sub>	$1.24 \times 10^{-16}$	-0.262
Cd <sub>R</sub>	$5.15 \times 10^{-16}$	0.256	ANG <sub>R</sub>	$2.89 \times 10^{-11}$	-0.210
Acb <sub>L</sub>	0.0158	0.0763	MD <sub>L</sub>	0.195	-0.0410
Acb <sub>R</sub>	$2.88 \times 10^{-8}$	0.176	MD <sub>R</sub>	0.0804	-0.0553
EA <sub>L</sub>	$1.02 \times 10^{-30}$	0.364	IML <sub>L</sub>	$4.16 \times 10^{-11}$	-0.209
EA <sub>R</sub>	$1.00 \times 10^{-32}$	0.377	IML <sub>R</sub>	$6.54 \times 10^{-16}$	-0.256
GPe <sub>L</sub>	$2.29 \times 10^{-34}$	0.387	LNG <sub>L</sub>	$6.78 \times 10^{-29}$	-0.353
GPe <sub>R</sub>	$5.57 \times 10^{-34}$	0.384	LNG <sub>R</sub>	$9.04 \times 10^{-30}$	-0.358
GPI <sub>L</sub>	$7.19 \times 10^{-36}$	0.395	Pul <sub>L</sub>	0.108	0.0508
GPI <sub>R</sub>	$2.87 \times 10^{-35}$	0.392	Pul <sub>R</sub>	$6.84 \times 10^{-6}$	0.142
SNr <sub>L</sub>	$7.76 \times 10^{-28}$	0.346	DN <sub>L</sub>	$2.65 \times 10^{-20}$	0.292
SNr <sub>R</sub>	$4.35 \times 10^{-29}$	0.354	DN <sub>R</sub>	$1.39 \times 10^{-18}$	0.278

Table 4.3: Results of Wilcoxon rank-sum test on QSM data of AD and non-AD groups in deep gray matter regions reconstructed using STAR-QSM. L/R subscript denotes left or right side.  $r_{rb}$  is the rank-biserial correlation

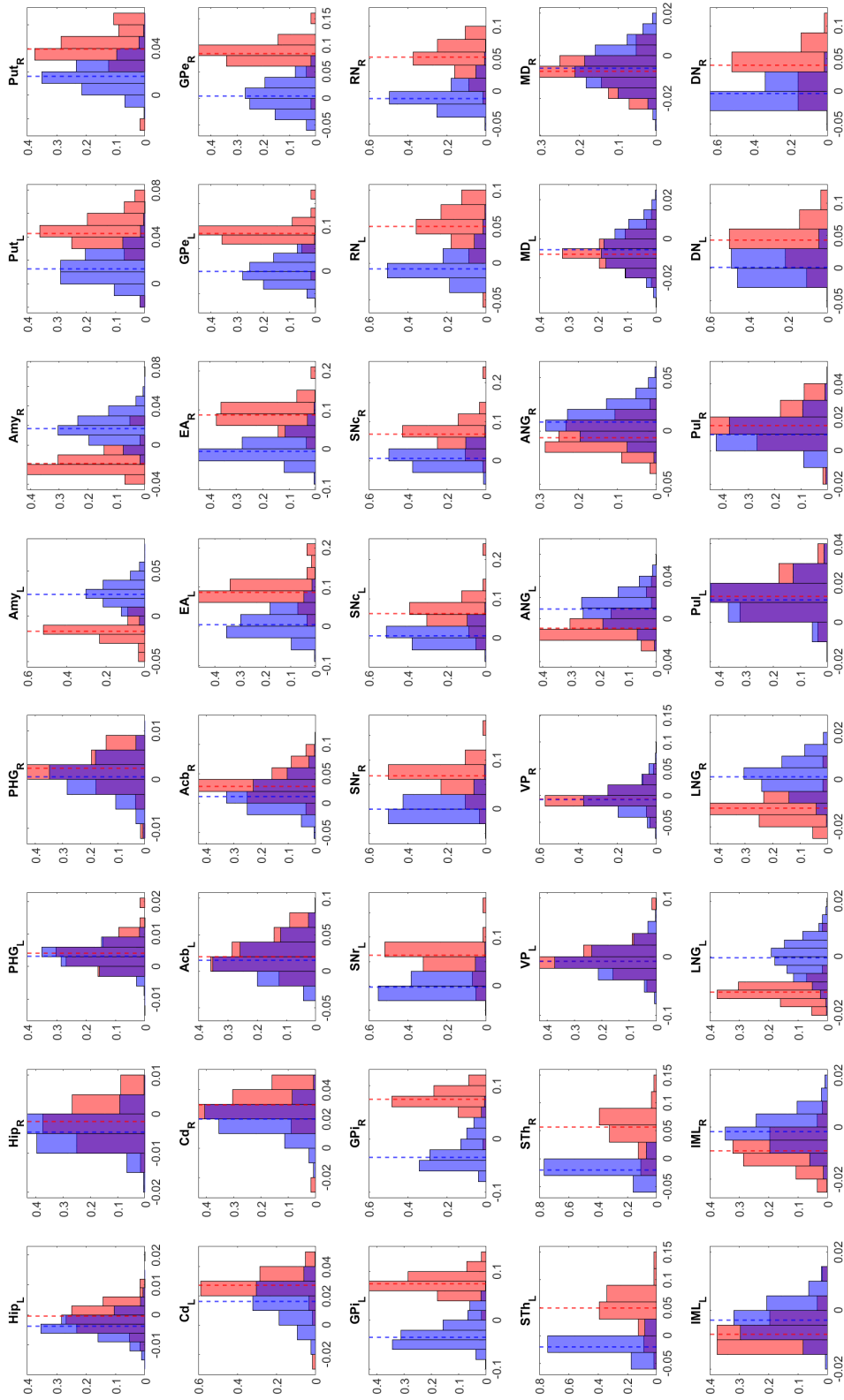


Figure 4.3: Proportion of participants with QSM signal in ppm (STAR-QSM reconstruction) in deep gray matter regions (Red: participants with AD diagnosis; blue: participants without AD diagnosis; dashed lines: medians of each group)

**68–75 Year Old Subsample**

Using data from participants within the 68–75 year old age range yields slightly different results with largely similar patterns. Compared to the entire sample, the differences between the AD and non-AD groups are more pronounced overall. Using either reconstruction method yields similar results.

ROI	$p$ -value	$r_{rb}$	ROI	$p$ -value	$r_{rb}$
Hip <sub>L</sub>	$1.18 \times 10^{-3}$	0.183	SN <sub>C</sub> <sub>L</sub>	$4.06 \times 10^{-15}$	0.442
Hip <sub>R</sub>	$2.16 \times 10^{-5}$	0.239	SN <sub>C</sub> <sub>R</sub>	$2.21 \times 10^{-16}$	0.462
PHG <sub>L</sub>	0.806	-0.0139	RN <sub>L</sub>	$3.48 \times 10^{-17}$	0.474
PHG <sub>R</sub>	$5.97 \times 10^{-3}$	0.155	RN <sub>R</sub>	$4.52 \times 10^{-18}$	0.488
Amy <sub>L</sub>	$1.14 \times 10^{-17}$	-0.482	STh <sub>L</sub>	$2.56 \times 10^{-17}$	0.476
Amy <sub>R</sub>	$5.89 \times 10^{-15}$	-0.439	STh <sub>R</sub>	$9.07 \times 10^{-17}$	0.468
Put <sub>L</sub>	$2.51 \times 10^{-14}$	0.429	VP <sub>L</sub>	0.240	0.0661
Put <sub>R</sub>	$2.09 \times 10^{-13}$	0.413	VP <sub>R</sub>	0.304	0.0579
Cd <sub>L</sub>	$9.10 \times 10^{-12}$	0.384	ANG <sub>L</sub>	$5.64 \times 10^{-8}$	-0.306
Cd <sub>R</sub>	$3.02 \times 10^{-8}$	0.312	ANG <sub>R</sub>	$3.16 \times 10^{-4}$	-0.203
Acb <sub>L</sub>	$2.87 \times 10^{-3}$	0.168	MD <sub>L</sub>	0.826	0.0124
Acb <sub>R</sub>	$2.08 \times 10^{-6}$	0.267	MD <sub>R</sub>	0.0545	-0.108
EA <sub>L</sub>	$1.89 \times 10^{-15}$	0.447	IML <sub>L</sub>	$2.50 \times 10^{-3}$	-0.170
EA <sub>R</sub>	$9.74 \times 10^{-17}$	0.467	IML <sub>R</sub>	$7.05 \times 10^{-7}$	-0.279
GPe <sub>L</sub>	$5.19 \times 10^{-17}$	0.472	LNG <sub>L</sub>	$3.55 \times 10^{-15}$	-0.443
GPe <sub>R</sub>	$1.03 \times 10^{-16}$	0.467	LNG <sub>R</sub>	$3.26 \times 10^{-15}$	-0.443
GPI <sub>L</sub>	$1.52 \times 10^{-18}$	0.494	Pul <sub>L</sub>	0.0349	0.119
GPI <sub>R</sub>	$2.39 \times 10^{-18}$	0.492	Pul <sub>R</sub>	$2.20 \times 10^{-5}$	0.239
SNr <sub>L</sub>	$3.37 \times 10^{-16}$	0.459	DN <sub>L</sub>	$4.90 \times 10^{-13}$	0.407
SNr <sub>R</sub>	$1.27 \times 10^{-16}$	0.466	DN <sub>R</sub>	$2.03 \times 10^{-14}$	0.430

Table 4.4: Results of Wilcoxon rank-sum test on QSM data of AD and non-AD groups (68–75 year old participants only) in deep gray matter regions reconstructed using iLSQR. L/R subscript denotes left or right side.  $r_{rb}$  is the rank-biserial correlation

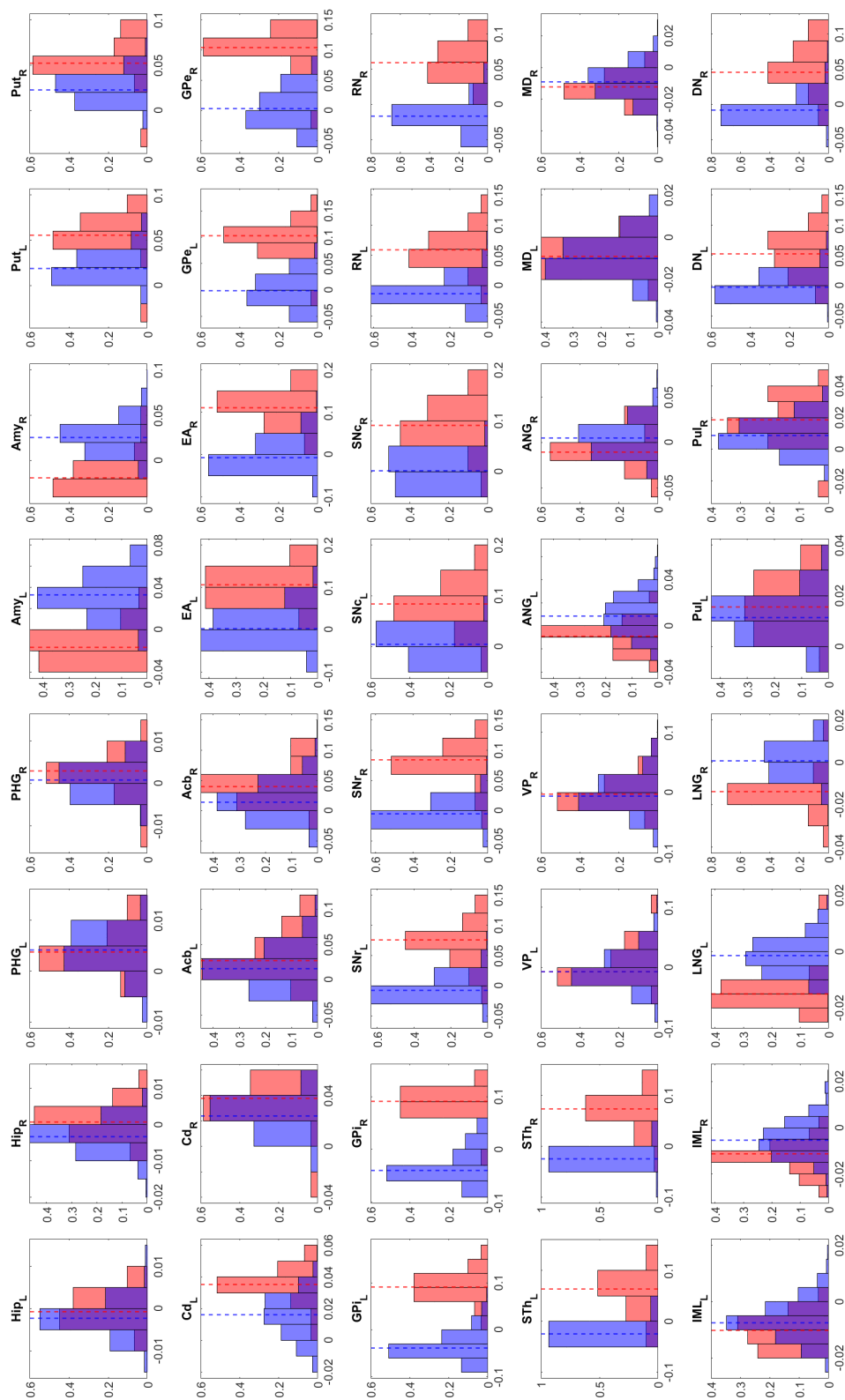


Figure 4.4: Proportion of 68–75 year old participants with QSM signal in ppm (iLSQR reconstruction) in deep gray matter regions (Red: participants with AD diagnosis; blue: participants without AD diagnosis; dashed lines: medians of each group)

## Aging Effects

We observe linear trends in the QSM of deep gray matter regions with respect to age in the non-AD group (Figure 4.3). Compared to the non-AD group, the distribution of QSM in the AD group has higher variance overall.

### Normal Aging Effects

Having observed linear trends in the non-AD group, we compute Pearson's  $r$  for each ROI to assess the linear relationship between age and QSM. There is again asymmetry between the two brain hemispheres.

ROI	$p$ -value	Pearson's $r$	ROI	$p$ -value	Pearson's $r$
Hip <sub>L</sub>	$1.15 \times 10^{-4}$	0.592	SN <sub>CL</sub>	$8.16 \times 10^{-3}$	0.428
Hip <sub>R</sub>	$1.93 \times 10^{-6}$	0.694	SN <sub>CR</sub>	0.0720	0.299
PHG <sub>L</sub>	0.259	0.191	RN <sub>L</sub>	0.392	0.145
PHG <sub>R</sub>	0.0573	0.315	RN <sub>R</sub>	0.987	0.00285
Amy <sub>L</sub>	0.715	-0.0622	STh <sub>L</sub>	0.0441	-0.333
Amy <sub>R</sub>	0.613	0.0860	STh <sub>R</sub>	0.0490	-0.326
Put <sub>L</sub>	$4.77 \times 10^{-4}$	-0.546	VP <sub>L</sub>	0.124	0.258
Put <sub>R</sub>	$5.82 \times 10^{-3}$	-0.445	VP <sub>R</sub>	$1.17 \times 10^{-3}$	0.513
Cd <sub>L</sub>	$4.19 \times 10^{-16}$	-0.923	ANG <sub>L</sub>	$6.11 \times 10^{-5}$	0.610
Cd <sub>R</sub>	$4.02 \times 10^{-12}$	-0.867	ANG <sub>R</sub>	0.212	0.210
Acb <sub>L</sub>	$6.93 \times 10^{-10}$	-0.817	MD <sub>L</sub>	$2.63 \times 10^{-5}$	-0.633
Acb <sub>R</sub>	$6.71 \times 10^{-11}$	-0.842	MD <sub>R</sub>	$3.16 \times 10^{-6}$	-0.683
EA <sub>L</sub>	$1.08 \times 10^{-8}$	-0.782	IML <sub>L</sub>	0.427	-0.135
EA <sub>R</sub>	$2.31 \times 10^{-10}$	-0.829	IML <sub>R</sub>	$8.33 \times 10^{-3}$	-0.427
GPe <sub>L</sub>	$8.92 \times 10^{-13}$	-0.879	LNG <sub>L</sub>	$1.37 \times 10^{-3}$	0.507
GPe <sub>R</sub>	$1.07 \times 10^{-12}$	-0.877	LNG <sub>R</sub>	$2.15 \times 10^{-3}$	0.489
GPI <sub>L</sub>	$6.83 \times 10^{-11}$	-0.842	Pul <sub>L</sub>	$4.19 \times 10^{-5}$	-0.621
GPI <sub>R</sub>	$2.97 \times 10^{-8}$	-0.768	Pul <sub>R</sub>	$2.13 \times 10^{-8}$	-0.773
SN <sub>L</sub>	0.174	0.228	DN <sub>L</sub>	$1.65 \times 10^{-3}$	-0.500
SN <sub>R</sub>	0.743	0.0558	DN <sub>R</sub>	$2.25 \times 10^{-3}$	-0.487

Table 4.5: Pearson correlation coefficient between the age and QSM data of participants without an AD diagnosis in deep gray matter regions reconstructed using iLSQR averaged by age. L/R subscript denotes left or right side

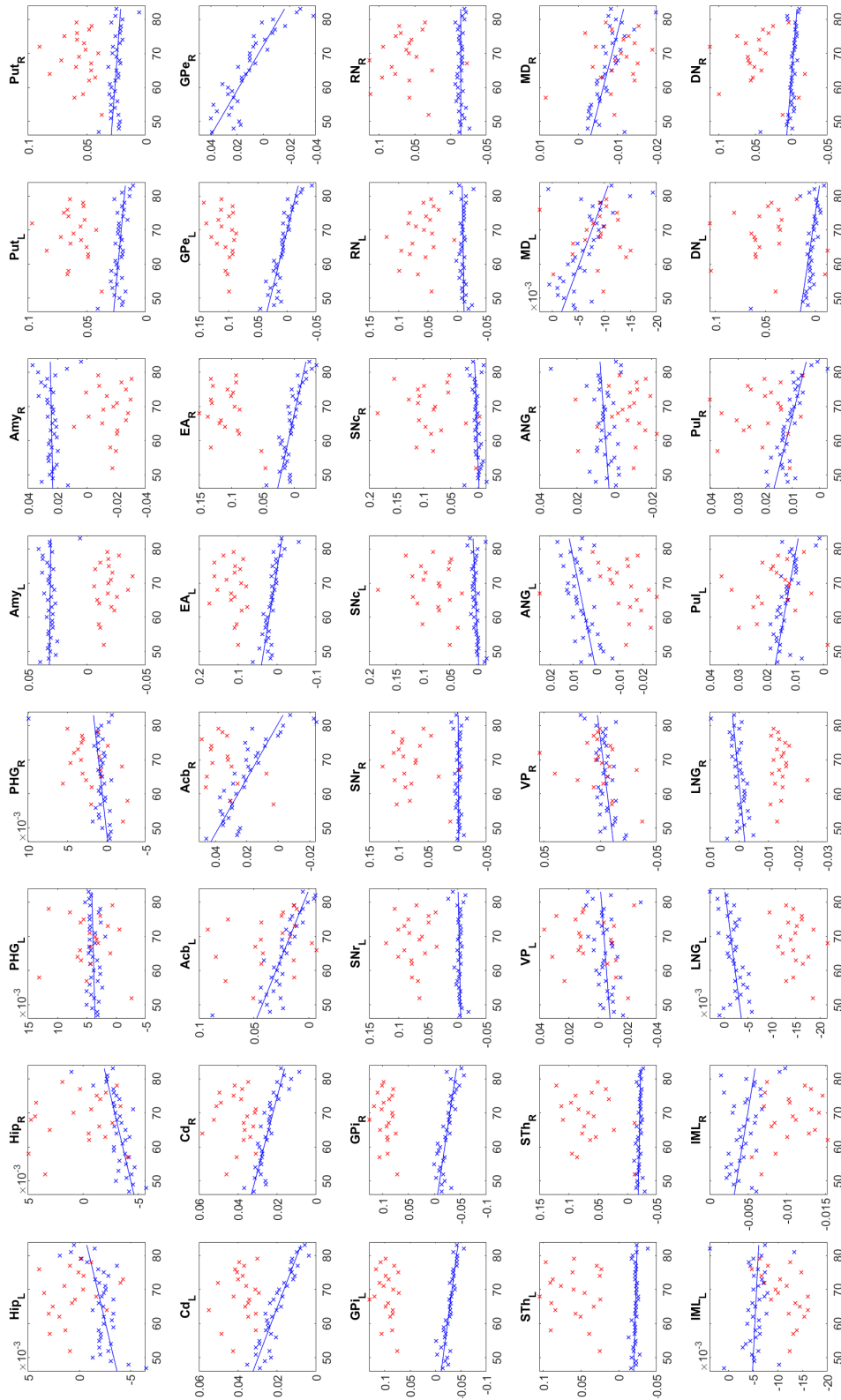


Figure 4-5: QSM signal in ppm (iLSQR reconstruction) in deep gray matter regions averaged by age (Red: participants with AD diagnosis; blue: participants without AD diagnosis. Line: least-squares of non-AD group)



## 4.6 Discussion

The results corroborate the findings of previous studies that pathological QSM patterns are observed in deep gray matter regions in AD, supporting the hypotheses that some form of iron dyshomeostasis is present in AD and that iron deposition occurs in AD. Given these clear pathological patterns, QSM may prove useful in the clinical setting as an auxiliary tool for AD diagnosis and research.

We find that QSM is asymmetric between the two brain hemispheres. This is plausible since brains are not completely symmetric both in terms of structure and function, and such observations have been previously reported ([18]).

There is a vast literature on how QSM of deep gray matter regions normally evolves with age ([37]). Iron is necessary for healthy childhood development, during which the QSM of these regions has been observed to increase ([11, 62, 63]). Beyond adolescence, this rising trend has been observed to mostly keep increasing into old age across all regions, but it can also plateau or even reverse slightly for particular regions ([13, 21, 30, 63]). We observe linear trends in both increasing and decreasing directions as well as plateaus in different deep gray matter regions. Our study contributes more data towards elucidating these trends.

## Chapter 5

# Is There a Connection Between Diet and QSM?

As diet does not seem to directly contribute to risk of AD based on our work, we would like to take a step back and explore whether there is a connection between diet and QSM.

We conduct an exploratory analysis by taking each of 33 numerical features in the dietary dataset (excluding sex and ethnicity) and the QSM of each of 40 deep gray matter regions to compute the Pearson correlation coefficient, only using data from participants who had a consistent diet as defined in Chapter 2. We use the Bonferroni adjustment to control false discovery rate. The sample included 14 participants with an AD diagnosis and 380 participants without an AD diagnosis.

No significant correlations involving dietary or lifestyle features were present, both in the AD group and the non-AD group. For the non-AD group, anthropometry measures were at most mildly correlated with QSM of only a couple of deep gray matter regions. As discussed in the previous chapter, out of all the features used for the dietary analysis, age was the most outstandingly correlated with QSM of deep gray matter regions for the non-AD group.

Our results suggest that diet may not be connected to regulatory processes in the brain that are related to iron.

**Age at Initial Assessment and QSM**

ROI	<i>p</i> -value	Pearson's <i>r</i>	ROI	<i>p</i> -value	Pearson's <i>r</i>
Hip <sub>L</sub>	0.139	0.0761	SN <sub>cL</sub>	0.0573	0.0976
Hip <sub>R</sub>	0.0241	0.116	SN <sub>cR</sub>	0.00213	0.157
PHG <sub>L</sub>	0.388	0.0444	RN <sub>L</sub>	0.575	0.0288
PHG <sub>R</sub>	0.495	-0.0351	RN <sub>R</sub>	0.776	-0.0146
Amy <sub>L</sub>	0.924	0.00491	STh <sub>L</sub>	0.395	-0.0438
Amy <sub>R</sub>	0.982	0.00118	STh <sub>R</sub>	0.154	-0.0732
Put <sub>L</sub>	0.0970	-0.0852	VP <sub>L</sub>	0.272	-0.0565
Put <sub>R</sub>	0.0109	-0.130	VP <sub>R</sub>	0.728	-0.0179
Cd <sub>L</sub>	$2.01 \times 10^{-14}$	-0.379	ANG <sub>L</sub>	0.331	0.0500
Cd <sub>R</sub>	$5.35 \times 10^{-10}$	-0.312	ANG <sub>R</sub>	0.00582	0.141
Acb <sub>L</sub>	$8.33 \times 10^{-9}$	-0.290	MD <sub>L</sub>	$6.07 \times 10^{-8}$	-0.273
Acb <sub>R</sub>	$4.15 \times 10^{-9}$	-0.296	MD <sub>R</sub>	$1.89 \times 10^{-4}$	-0.190
EA <sub>L</sub>	$2.68 \times 10^{-6}$	-0.238	IML <sub>L</sub>	0.139	-0.0760
EA <sub>R</sub>	$2.73 \times 10^{-5}$	-0.213	IML <sub>R</sub>	0.429	-0.0407
GPe <sub>L</sub>	$4.41 \times 10^{-7}$	-0.256	LNG <sub>L</sub>	0.00349	0.149
GPe <sub>R</sub>	$5.72 \times 10^{-11}$	-0.328	LNG <sub>R</sub>	0.00668	0.139
GPi <sub>L</sub>	$1.51 \times 10^{-4}$	-0.193	Pul <sub>L</sub>	$1.90 \times 10^{-4}$	-0.190
GPi <sub>R</sub>	$1.33 \times 10^{-6}$	-0.245	Pul <sub>R</sub>	$2.40 \times 10^{-6}$	-0.239
SN <sub>rL</sub>	0.908	0.00598	DN <sub>L</sub>	$4.43 \times 10^{-5}$	-0.208
SN <sub>rR</sub>	0.615	0.0259	DN <sub>R</sub>	$1.22 \times 10^{-4}$	-0.196

Table 5.1: Pearson correlation coefficient between the age at the initial assessment visit and QSM data of participants with a consistent diet and without an AD diagnosis in deep gray matter regions reconstructed using iLSQR. L/R subscript denotes left or right side

### Body Mass Index and QSM

We give body mass index as an example of an anthropometry measure that has few significant correlations with QSM.

ROI	$p$ -value	Pearson's $r$	ROI	$p$ -value	Pearson's $r$
Hip <sub>L</sub>	0.602	-0.0269	SN <sub>C<sub>L</sub></sub>	0.157	-0.0727
Hip <sub>R</sub>	0.799	0.0131	SN <sub>C<sub>R</sub></sub>	0.583	0.0283
PHG <sub>L</sub>	0.00929	-0.133	RN <sub>L</sub>	0.189	-0.0675
PHG <sub>R</sub>	0.606	-0.0265	RN <sub>R</sub>	0.382	-0.0450
Amy <sub>L</sub>	0.677	-0.0214	STh <sub>L</sub>	0.0226	-0.117
Amy <sub>R</sub>	0.542	-0.0314	STh <sub>R</sub>	0.0218	-0.118
Put <sub>L</sub>	0.0701	-0.0930	VP <sub>L</sub>	0.580	-0.0285
Put <sub>R</sub>	0.590	-0.0277	VP <sub>R</sub>	0.365	0.0466
Cd <sub>L</sub>	0.00285	-0.153	ANG <sub>L</sub>	0.159	0.0723
Cd <sub>R</sub>	0.352	-0.0478	ANG <sub>R</sub>	0.210	-0.0645
Acb <sub>L</sub>	0.00363	-0.149	MD <sub>L</sub>	0.0649	-0.0948
Acb <sub>R</sub>	0.229	-0.0619	MD <sub>R</sub>	0.00901	-0.134
EA <sub>L</sub>	0.433	-0.0404	IML <sub>L</sub>	0.306	-0.0526
EA <sub>R</sub>	0.552	-0.0306	IML <sub>R</sub>	0.188	-0.0677
GPe <sub>L</sub>	0.251	-0.0590	LNG <sub>L</sub>	0.716	-0.0187
GPe <sub>R</sub>	0.554	-0.0304	LNG <sub>R</sub>	0.103	0.0838
GPI <sub>L</sub>	0.364	0.0467	Pul <sub>L</sub>	0.560	-0.0300
GPI <sub>R</sub>	0.983	0.00109	Pul <sub>R</sub>	0.150	0.0740
SNr <sub>L</sub>	0.114	-0.0813	DN <sub>L</sub>	$9.83 \times 10^{-6}$	-0.225
SNr <sub>R</sub>	0.983	-0.00107	DN <sub>R</sub>	$9.61 \times 10^{-5}$	-0.199

Table 5.2: Pearson correlation coefficient between the Body Mass Index and QSM data of participants with a consistent diet and without an AD diagnosis in deep gray matter regions reconstructed using iLSQR. L/R subscript denotes left or right side

### Alcohol Intake Frequency and QSM

We give alcohol intake frequency as an example of a dietary feature that does not have any significant correlations with QSM.

ROI	$p$ -value	Pearson's $r$	ROI	$p$ -value	Pearson's $r$
Hip <sub>L</sub>	0.262	-0.0577	SN <sub>C</sub> <sub>L</sub>	0.120	-0.0800
Hip <sub>R</sub>	0.0533	-0.0992	SN <sub>C</sub> <sub>R</sub>	0.0763	-0.0911
PHG <sub>L</sub>	0.871	-0.00839	RN <sub>L</sub>	0.444	-0.0394
PHG <sub>R</sub>	0.234	0.0612	RN <sub>R</sub>	0.393	-0.0439
Amy <sub>L</sub>	0.909	0.00586	STh <sub>L</sub>	0.503	-0.0345
Amy <sub>R</sub>	0.801	-0.0130	STh <sub>R</sub>	0.943	-0.00369
Put <sub>L</sub>	0.484	-0.0360	VP <sub>L</sub>	0.136	0.0767
Put <sub>R</sub>	0.0979	-0.0850	VP <sub>R</sub>	0.282	0.0553
Cd <sub>L</sub>	0.0240	0.116	ANG <sub>L</sub>	0.250	-0.0592
Cd <sub>R</sub>	0.288	0.0546	ANG <sub>R</sub>	0.152	-0.0735
Acb <sub>L</sub>	0.186	0.0680	MD <sub>L</sub>	0.416	0.0418
Acb <sub>R</sub>	0.193	0.0669	MD <sub>R</sub>	0.0332	0.109
EA <sub>L</sub>	0.443	0.0395	IML <sub>L</sub>	0.926	-0.00481
EA <sub>R</sub>	0.0708	0.0928	IML <sub>R</sub>	0.106	0.0832
GPe <sub>L</sub>	0.424	0.0411	LNG <sub>L</sub>	0.472	0.0370
GPe <sub>R</sub>	0.368	0.0464	LNG <sub>R</sub>	0.481	-0.0363
GPI <sub>L</sub>	0.636	0.0244	Pul <sub>L</sub>	0.735	0.0174
GPI <sub>R</sub>	0.219	0.0631	Pul <sub>R</sub>	0.416	0.0419
SN <sub>r</sub> <sub>L</sub>	0.275	-0.0562	DN <sub>L</sub>	0.0472	0.102
SN <sub>r</sub> <sub>R</sub>	0.377	-0.0454	DN <sub>R</sub>	0.724	0.0182

Table 5.3: Pearson correlation coefficient between the alcohol intake frequency (aggregated across all responses) and QSM data of participants with a consistent diet and without an AD diagnosis in deep gray matter regions reconstructed using iLSQR. L/R subscript denotes left or right side

# Chapter 6

## Conclusion

### 6.1 Future Work

We have not explored fully what UK Biobank has to offer. For instance, blood samples provide information that is downstream from diet and upstream of iron deposition. We could also broaden the scope to all-cause dementia and other neurodegenerative diseases. When the UK Biobank cognitive battery is established to be more reliable, we could use it to screen for cognitive deficits instead of only relying on formal diagnoses.

As UK Biobank continues to collect more data from the cohort, we are certain this will enable more interesting and impactful studies in the years to come, such as longitudinal studies using QSM data. It is possible that those who have developed AD for a longer time have more distinctive QSM patterns as pathological features have had more time to manifest.

### 6.2 Iron in AD Pathology

The detection of iron in the brain, like other biomarkers in AD, does not imply any causal relationship between its deposition and the development of the disease. There is speculation what exactly leads to iron deposition and how iron deposition is linked to neurodegeneration. Our results suggest that dietary lifestyle habits may not be risk factors for AD and corroborate the popular hypothesis that processes regulating iron are dysfunctional in AD.

# Bibliography

- [1] C. W. Adams. “Perivascular Iron Deposition and Other Vascular Damage in Multiple Sclerosis”. In: *Journal of Neurology, Neurosurgery, and Psychiatry* 51.2 (Feb. 1988), pp. 260–265. ISSN: 0022-3050. DOI: [10.1136/jnnp.51.2.260](https://doi.org/10.1136/jnnp.51.2.260).
- [2] Fidel Alfaro-Almagro et al. “Image Processing and Quality Control for the First 10,000 Brain Imaging Datasets from UK Biobank”. In: *NeuroImage* 166 (Feb. 2018), pp. 400–424. ISSN: 1095-9572. DOI: [10.1016/j.neuroimage.2017.10.034](https://doi.org/10.1016/j.neuroimage.2017.10.034).
- [3] Azhaar Ashraf et al. “Iron Dyshomeostasis, Lipid Peroxidation and Perturbed Expression of Cystine/Glutamate Antiporter in Alzheimer’s Disease: Evidence of Ferroptosis”. In: *Redox Biology* 32 (May 2020), p. 101494. ISSN: 2213-2317. DOI: [10.1016/j.redox.2020.101494](https://doi.org/10.1016/j.redox.2020.101494).
- [4] B. B. Avants et al. “Symmetric Diffeomorphic Image Registration with Cross-Correlation: Evaluating Automated Labeling of Elderly and Neurodegenerative Brain”. In: *Medical Image Analysis* 12.1 (Feb. 2008), pp. 26–41. ISSN: 1361-8423. DOI: [10.1016/j.media.2007.06.004](https://doi.org/10.1016/j.media.2007.06.004).
- [5] Scott Ayton et al. “Brain Iron Is Associated with Accelerated Cognitive Decline in People with Alzheimer Pathology”. In: *Molecular psychiatry* 25.11 (Nov. 2020), pp. 2932–2941. ISSN: 1359-4184. DOI: [10.1038/s41380-019-0375-7](https://doi.org/10.1038/s41380-019-0375-7).
- [6] Scott Ayton et al. “Parkinson’s Disease Iron Deposition Caused by Nitric Oxide-Induced Loss of  $\beta$ -Amyloid Precursor Protein”. In: *The Journal of Neuroscience* 35.8 (Feb. 2015), pp. 3591–3597. ISSN: 0270-6474. DOI: [10.1523/JNEUROSCI.3439-14.2015](https://doi.org/10.1523/JNEUROSCI.3439-14.2015).
- [7] Gérard Biau, Luc Devroye, and Gábor Lugosi. “Consistency of Random Forests and Other Averaging Classifiers”. In: *Journal of Machine Learning Research* 9.66 (2008), pp. 2015–2033. ISSN: 1533-7928. URL: <http://jmlr.org/papers/v9/biau08a.html>.
- [8] UK Biobank. *Repeat Assessment: Participant Characteristics of Responders vs. Non-Responders*. July 2014. URL: [https://biobank.ndph.ox.ac.uk/~bbdatan/repeat\\_assessment\\_characteristics\\_v1.pdf](https://biobank.ndph.ox.ac.uk/~bbdatan/repeat_assessment_characteristics_v1.pdf).
- [9] Leo Breiman. “Random Forests”. In: *Machine Learning* 45.1 (Oct. 2001), pp. 5–32. ISSN: 1573-0565. DOI: [10.1023/A:1010933404324](https://doi.org/10.1023/A:1010933404324).

- [10] Leo Breiman et al. *Classification and Regression Trees*. Taylor & Francis, Jan. 1984. ISBN: 978-0-412-04841-8.
- [11] Kimberly L. H. Carpenter et al. “Magnetic Susceptibility of Brain Iron Is Associated with Childhood Spatial IQ”. In: *NeuroImage* 132 (May 2016), pp. 167–174. ISSN: 1053-8119. DOI: [10.1016/j.neuroimage.2016.02.028](https://doi.org/10.1016/j.neuroimage.2016.02.028).
- [12] Rudy J. Castellani et al. “Iron: The Redox-active Center of Oxidative Stress in Alzheimer Disease”. In: *Neurochemical Research* 32.10 (Oct. 2007), pp. 1640–1645. ISSN: 1573-6903. DOI: [10.1007/s11064-007-9360-7](https://doi.org/10.1007/s11064-007-9360-7).
- [13] Gloria C Chiang et al. “Brain Oxygen Extraction and Neural Tissue Susceptibility Are Associated with Cognitive Impairment in Older Individuals”. In: *Journal of neuroimaging : official journal of the American Society of Neuroimaging* 32.4 (July 2022), pp. 697–709. ISSN: 1051-2284. DOI: [10.1111/jon.12990](https://doi.org/10.1111/jon.12990).
- [14] Scott J. Dixon et al. “Ferroptosis: An Iron-Dependent Form of Nonapoptotic Cell Death”. In: *Cell* 149.5 (May 2012), pp. 1060–1072. ISSN: 0092-8674, 1097-4172. DOI: [10.1016/j.cell.2012.03.042](https://doi.org/10.1016/j.cell.2012.03.042).
- [15] Chloe Fawns-Ritchie and Ian J. Deary. “Reliability and Validity of the UK Biobank Cognitive Tests”. In: *PLoS ONE* 15.4 (Apr. 2020), e0231627. ISSN: 1932-6203. DOI: [10.1371/journal.pone.0231627](https://doi.org/10.1371/journal.pone.0231627).
- [16] Anna Fry et al. “Comparison of Sociodemographic and Health-Related Characteristics of UK Biobank Participants With Those of the General Population”. In: *American Journal of Epidemiology* 186.9 (Nov. 2017), pp. 1026–1034. ISSN: 1476-6256. DOI: [10.1093/aje/kwx246](https://doi.org/10.1093/aje/kwx246).
- [17] Andrew Gleason and Ashley I. Bush. “Iron and Ferroptosis as Therapeutic Targets in Alzheimer’s Disease”. In: *Neurotherapeutics* 18.1 (Jan. 2021), pp. 252–264. ISSN: 1933-7213. DOI: [10.1007/s13311-020-00954-y](https://doi.org/10.1007/s13311-020-00954-y).
- [18] Nan-Jie Gong et al. “Hemisphere, Gender and Age-Related Effects on Iron Deposition in Deep Gray Matter Revealed by Quantitative Susceptibility Mapping”. In: *NMR in biomedicine* 28.10 (Oct. 2015), pp. 1267–1274. ISSN: 1099-1492. DOI: [10.1002/nbm.3366](https://doi.org/10.1002/nbm.3366).
- [19] Xiaojun Guan et al. “Altered Brain Iron Depositions from Aging to Parkinson’s Disease and Alzheimer’s Disease: A Quantitative Susceptibility Mapping Study”. In: *NeuroImage* 264 (Dec. 2022), p. 119683. ISSN: 1053-8119. DOI: [10.1016/j.neuroimage.2022.119683](https://doi.org/10.1016/j.neuroimage.2022.119683).
- [20] Trevor Hastie, Robert Tibshirani, and Jerome Friedman. *The Elements of Statistical Learning*. Springer Series in Statistics. New York, NY: Springer, 2009. ISBN: 978-0-387-84858-7. DOI: [10.1007/978-0-387-84858-7](https://doi.org/10.1007/978-0-387-84858-7).
- [21] Courtney M. Howard et al. “Cortical Iron Mediates Age-Related Decline in Fluid Cognition”. In: *Human Brain Mapping* 43.3 (2022), pp. 1047–1060. ISSN: 1097-0193. DOI: [10.1002/hbm.25706](https://doi.org/10.1002/hbm.25706).



- [22] Laurent Hyafil and Ronald L. Rivest. “Constructing Optimal Binary Decision Trees Is NP-complete”. In: *Information Processing Letters* 5.1 (May 1976), pp. 15–17. ISSN: 0020-0190. DOI: [10.1016/0020-0190\(76\)90095-8](https://doi.org/10.1016/0020-0190(76)90095-8).
- [23] Mark Jenkinson et al. “FSL”. In: *NeuroImage* 62.2 (Aug. 2012), pp. 782–790. ISSN: 1095-9572. DOI: [10.1016/j.neuroimage.2011.09.015](https://doi.org/10.1016/j.neuroimage.2011.09.015).
- [24] Hong Jiang et al. “Iron Pathophysiology in Parkinson Diseases”. In: *Brain Iron Metabolism and CNS Diseases*. Ed. by Yan-Zhong Chang. Advances in Experimental Medicine and Biology. Singapore: Springer, 2019, pp. 45–66. ISBN: 9789811395895. DOI: [10.1007/978-981-13-9589-5\\_4](https://doi.org/10.1007/978-981-13-9589-5_4).
- [25] J. P. Kehrer. “The Haber-Weiss Reaction and Mechanisms of Toxicity”. In: *Toxicology* 149.1 (Aug. 2000), pp. 43–50. ISSN: 0300-483X. DOI: [10.1016/s0300-483x\(00\)00231-6](https://doi.org/10.1016/s0300-483x(00)00231-6).
- [26] Michael Khalil, Charlotte Teunissen, and Christian Langkammer. “Iron and Neurodegeneration in Multiple Sclerosis”. In: *Multiple Sclerosis International* 2011 (2011), p. 606807. ISSN: 2090-2654. DOI: [10.1155/2011/606807](https://doi.org/10.1155/2011/606807).
- [27] Darius J. R. Lane, Scott Ayton, and Ashley I. Bush. “Iron and Alzheimer’s Disease: An Update on Emerging Mechanisms”. In: *Journal of Alzheimer’s Disease* 64.s1 (Jan. 2018), S379–S395. ISSN: 1387-2877. DOI: [10.3233/JAD-179944](https://doi.org/10.3233/JAD-179944).
- [28] Wei Li, Bing Wu, and Chunlei Liu. “Quantitative Susceptibility Mapping of Human Brain Reflects Spatial Variation in Tissue Composition”. In: *NeuroImage* 55.4 (Apr. 2011), pp. 1645–1656. ISSN: 1053-8119. DOI: [10.1016/j.neuroimage.2010.11.088](https://doi.org/10.1016/j.neuroimage.2010.11.088).
- [29] Wei Li et al. “A Method for Estimating and Removing Streaking Artifacts in Quantitative Susceptibility Mapping”. In: *NeuroImage* 108 (Mar. 2015), pp. 111–122. ISSN: 1053-8119. DOI: [10.1016/j.neuroimage.2014.12.043](https://doi.org/10.1016/j.neuroimage.2014.12.043).
- [30] Wei Li et al. “Differential Developmental Trajectories of Magnetic Susceptibility in Human Brain Gray and White Matter over the Lifespan”. In: *Human Brain Mapping* 35.6 (Sept. 2013), pp. 2698–2713. ISSN: 1065-9471. DOI: [10.1002/hbm.22360](https://doi.org/10.1002/hbm.22360).
- [31] Wei Li et al. “Integrated Laplacian-based Phase Unwrapping and Background Phase Removal for Quantitative Susceptibility Mapping”. In: *NMR in biomedicine* 27.2 (Feb. 2014), pp. 219–227. ISSN: 0952-3480. DOI: [10.1002/nbm.3056](https://doi.org/10.1002/nbm.3056).
- [32] Bette Liu et al. “Development and Evaluation of the Oxford WebQ, a Low-Cost, Web-Based Method for Assessment of Previous 24 h Dietary Intakes in Large-Scale Prospective Studies”. In: *Public Health Nutrition* 14.11 (Nov. 2011), pp. 1998–2005. ISSN: 1475-2727. DOI: [10.1017/S1368980011000942](https://doi.org/10.1017/S1368980011000942).
- [33] Chunlei Liu et al. “Quantitative Susceptibility Mapping: Contrast Mechanisms and Clinical Applications”. In: *Tomography* 1.1 (Sept. 2015), pp. 3–17. ISSN: 2379-1381. DOI: [10.18383/j.tom.2015.00136](https://doi.org/10.18383/j.tom.2015.00136).

- [34] Jiahao Liu et al. “The Association between Dietary Iron Intake and Incidence of Dementia in Adults Aged 60 Years or over in the UK Biobank”. In: *Nutrients* 15.2 (Jan. 2023), p. 260. ISSN: 2072-6643. DOI: [10.3390/nu15020260](https://doi.org/10.3390/nu15020260).
- [35] Jun-Lin Liu et al. “Iron and Alzheimer’s Disease: From Pathogenesis to Therapeutic Implications”. In: *Frontiers in Neuroscience* 12 (Sept. 2018), p. 632. ISSN: 1662-4548. DOI: [10.3389/fnins.2018.00632](https://doi.org/10.3389/fnins.2018.00632).
- [36] Giancarlo Logroscino et al. “Dietary Iron Intake and Risk of Parkinson’s Disease”. In: *American Journal of Epidemiology* 168.12 (Dec. 2008), pp. 1381–1388. ISSN: 0002-9262. DOI: [10.1093/aje/kwn273](https://doi.org/10.1093/aje/kwn273).
- [37] David J. Madden and Jenna L. Merenstein. “Quantitative Susceptibility Mapping of Brain Iron in Healthy Aging and Cognition”. In: *NeuroImage* 282 (Nov. 2023), p. 120401. ISSN: 1053-8119. DOI: [10.1016/j.neuroimage.2023.120401](https://doi.org/10.1016/j.neuroimage.2023.120401).
- [38] Kenneth E. L. McColl. “Effect of Proton Pump Inhibitors on Vitamins and Iron”. In: *Official journal of the American College of Gastroenterology — ACG* 104 (Mar. 2009), S5. ISSN: 0002-9270. URL: [https://journals.lww.com/ajg/Fulltext/2009/03002/Effect\\_of\\_Proton\\_Pump\\_Inhibitors\\_on\\_Vitamins\\_and.3.aspx](https://journals.lww.com/ajg/Fulltext/2009/03002/Effect_of_Proton_Pump_Inhibitors_on_Vitamins_and.3.aspx).
- [39] Karla L Miller et al. “Multimodal Population Brain Imaging in the UK Biobank Prospective Epidemiological Study”. In: *Nature neuroscience* 19.11 (Nov. 2016), pp. 1523–1536. ISSN: 1097-6256. DOI: [10.1038/nn.4393](https://doi.org/10.1038/nn.4393).
- [40] National Institute on Aging. *Alzheimer’s Disease Fact Sheet*. 2023. URL: <https://www.nia.nih.gov/health/alzheimers-and-dementia/alzheimers-disease-fact-sheet>.
- [41] Sara Nikseresht, Ashley I. Bush, and Scott Ayton. “Treating Alzheimer’s Disease by Targeting Iron”. In: *British Journal of Pharmacology* 176.18 (Sept. 2019), pp. 3622–3635. ISSN: 0007-1188. DOI: [10.1111/bph.14567](https://doi.org/10.1111/bph.14567).
- [42] Office for National Statistics. *2011 Census - Office for National Statistics*. URL: <https://www.ons.gov.uk/peoplepopulationandcommunity/populationandmigration/populationestimates/bulletins/2011censuspopulationestimatesfortheunitedkingdom/2012-12-17>.
- [43] Aurora Perez-Cornago et al. “Description of the Updated Nutrition Calculation of the Oxford WebQ Questionnaire and Comparison with the Previous Version among 207,144 Participants in UK Biobank”. In: *European Journal of Nutrition* 60.7 (Oct. 2021), pp. 4019–4030. ISSN: 1436-6215. DOI: [10.1007/s00394-021-02558-4](https://doi.org/10.1007/s00394-021-02558-4).
- [44] Elif Piskin et al. “Iron Absorption: Factors, Limitations, and Improvement Methods”. In: *ACS Omega* 7.24 (June 2022), pp. 20441–20456. ISSN: 2470-1343. DOI: [10.1021/acsomega.2c01833](https://doi.org/10.1021/acsomega.2c01833).
- [45] Tabea Schoeler et al. “Participation Bias in the UK Biobank Distorts Genetic Associations and Downstream Analyses”. In: *Nature Human Behaviour* 7.7 (July 2023), pp. 1216–1227. ISSN: 2397-3374. DOI: [10.1038/s41562-023-01579-9](https://doi.org/10.1038/s41562-023-01579-9).

- [46] Marvin A. Schofield and Yimei Zhu. “Fast Phase Unwrapping Algorithm for Interferometric Applications”. In: *Optics Letters* 28.14 (July 2003), pp. 1194–1196. ISSN: 0146-9592. DOI: [10.1364/ol.28.001194](https://doi.org/10.1364/ol.28.001194).
- [47] Ferdinand Schweser et al. “Quantitative Imaging of Intrinsic Magnetic Tissue Properties Using MRI Signal Phase: An Approach to in Vivo Brain Iron Metabolism?” In: *NeuroImage* 54.4 (Feb. 2011), pp. 2789–2807. ISSN: 1095-9572. DOI: [10.1016/j.neuroimage.2010.10.070](https://doi.org/10.1016/j.neuroimage.2010.10.070).
- [48] Erwan Scornet, Gérard Biau, and Jean-Philippe Vert. “Consistency of Random Forests”. In: *The Annals of Statistics* 43.4 (Aug. 2015). ISSN: 0090-5364. DOI: [10.1214/15-AOS1321](https://doi.org/10.1214/15-AOS1321). arXiv: [1405.2881 \[math, stat\]](https://arxiv.org/abs/1405.2881).
- [49] Zumin Shi et al. “High Iron Intake Is Associated with Poor Cognition among Chinese Old Adults and Varied by Weight Status—a 15-y Longitudinal Study in 4852 Adults”. In: *The American Journal of Clinical Nutrition* 109.1 (Jan. 2019), pp. 109–116. ISSN: 0002-9165. DOI: [10.1093/ajcn/nqy254](https://doi.org/10.1093/ajcn/nqy254).
- [50] Stephen Smith, Fidel Alfaro-Almagro, and Karla Miller. *Brain Imaging Documentation*. 2022.
- [51] Stephen M. Smith. “Fast Robust Automated Brain Extraction”. In: *Human Brain Mapping* 17.3 (Nov. 2002), pp. 143–155. ISSN: 1065-9471. DOI: [10.1002/hbm.10062](https://doi.org/10.1002/hbm.10062).
- [52] Cathie Sudlow et al. “UK Biobank: An Open Access Resource for Identifying the Causes of a Wide Range of Complex Diseases of Middle and Old Age”. In: *PLoS Medicine* 12.3 (Mar. 2015), e1001779. ISSN: 1549-1277. DOI: [10.1371/journal.pmed.1001779](https://doi.org/10.1371/journal.pmed.1001779).
- [53] Cheng Tang, Damien Garreau, and Ulrike von Luxburg. “When Do Random Forests Fail?” In: *Advances in Neural Information Processing Systems*. Vol. 31. Curran Associates, Inc., 2018. URL: [https://papers.nips.cc/paper\\_files/paper/2018/hash/204da255aea2cd4a75ace6018fad6b4d-Abstract.html](https://papers.nips.cc/paper_files/paper/2018/hash/204da255aea2cd4a75ace6018fad6b4d-Abstract.html).
- [54] Yunlong Tao et al. “Perturbed Iron Distribution in Alzheimer’s Disease Serum, Cerebrospinal Fluid, and Selected Brain Regions: A Systematic Review and Meta-Analysis”. In: *Journal of Alzheimer’s disease: JAD* 42.2 (2014), pp. 679–690. ISSN: 1875-8908. DOI: [10.3233/JAD-140396](https://doi.org/10.3233/JAD-140396).
- [55] George Edward Calver Thomas et al. “Brain Iron Deposition Is Linked with Cognitive Severity in Parkinson’s Disease”. In: *Journal of Neurology, Neurosurgery & Psychiatry* 91.4 (Apr. 2020), pp. 418–425. ISSN: 0022-3050, 1468-330X. DOI: [10.1136/jnnp-2019-322042](https://doi.org/10.1136/jnnp-2019-322042).
- [56] Sarah Treit et al. “R2\* and Quantitative Susceptibility Mapping in Deep Gray Matter of 498 Healthy Controls from 5 to 90 Years”. In: *Human Brain Mapping* 42.14 (June 2021), pp. 4597–4610. ISSN: 1065-9471. DOI: [10.1002/hbm.25569](https://doi.org/10.1002/hbm.25569).

- [57] Chaoyue Wang et al. “Phenotypic and Genetic Associations of Quantitative Magnetic Susceptibility in UK Biobank Brain Imaging”. In: *Nature Neuroscience* 25.6 (June 2022), pp. 818–831. ISSN: 1546-1726. DOI: [10.1038/s41593-022-01074-w](https://doi.org/10.1038/s41593-022-01074-w).
- [58] Feixue Wang et al. “Iron Dyshomeostasis and Ferroptosis: A New Alzheimer’s Disease Hypothesis?” In: *Frontiers in Aging Neuroscience* 14 (2022), p. 830569. ISSN: 1663-4365. DOI: [10.3389/fnagi.2022.830569](https://doi.org/10.3389/fnagi.2022.830569).
- [59] Tao Wang et al. “Iron Pathophysiology in Alzheimer’s Diseases”. In: *Brain Iron Metabolism and CNS Diseases*. Ed. by Yan-Zhong Chang. Advances in Experimental Medicine and Biology. Singapore: Springer, 2019, pp. 67–104. ISBN: 9789811395895. DOI: [10.1007/978-981-13-9589-5\\_5](https://doi.org/10.1007/978-981-13-9589-5_5).
- [60] Roberta J Ward et al. “The Role of Iron in Brain Ageing and Neurodegenerative Disorders”. In: *The Lancet. Neurology* 13.10 (Oct. 2014), pp. 1045–1060. ISSN: 1474-4422. DOI: [10.1016/S1474-4422\(14\)70117-6](https://doi.org/10.1016/S1474-4422(14)70117-6).
- [61] Hongjiang Wei et al. “Streaking Artifact Reduction for Quantitative Susceptibility Mapping of Sources with Large Dynamic Range”. In: *NMR in biomedicine* 28.10 (Oct. 2015), pp. 1294–1303. ISSN: 0952-3480. DOI: [10.1002/nbm.3383](https://doi.org/10.1002/nbm.3383).
- [62] Jerome Y. Yager and Dawn S. Hartfield. “Neurologic Manifestations of Iron Deficiency in Childhood”. In: *Pediatric Neurology* 27.2 (Aug. 2002), pp. 85–92. ISSN: 0887-8994, 1873-5150. DOI: [10.1016/S0887-8994\(02\)00417-4](https://doi.org/10.1016/S0887-8994(02)00417-4).
- [63] Yuyao Zhang et al. “Longitudinal Atlas for Normative Human Brain Development and Aging over the Lifespan Using Quantitative Susceptibility Mapping”. In: *NeuroImage* 171 (May 2018), pp. 176–189. ISSN: 1053-8119. DOI: [10.1016/j.neuroimage.2018.01.008](https://doi.org/10.1016/j.neuroimage.2018.01.008).